Experimental evaluation of manganese ores for chemical looping conversion of synthetic biomass volatiles in a 300 W reactor system

N.B. When citing this work, cite the original published paper.

(article starts on next page)

Experimental evaluation of manganese ores for chemical looping conversion of synthetic biomass volatiles in a 300 W reactor system

Ali Hedayati [*], Amir H. Soleimanisalim, Carl Johan Linderholm, Tobias Mattisson, Anders Lyngfelt

Chalmers University of Technology, Division of Energy Technology, Hörsalsvägen 7B, 412 58 Göteborg, Sweden

ARTICLE INFO

ABSTRACT

Two manganese ores with different iron content were investigated as oxygen carriers for chemical looping conversion of simulated biomass volatiles. The aim was to study the performance of the oxygen carriers with regards to combustion and potential use for chemical-looping gasification of wood-based biomass. The oxygen carriers were studied in a 300 W chemical-looping reactor system with circulation of oxygen carriers between the fluidized air and fuel reactors. The temperature was 850–900 °C and the fuel flow rates were 0.6–3 Lmin^{-1}. The Mn ore with higher iron content showed significant oxygen release at 900 °C under inert conditions, as well as full conversion of CO, H_2 and methane at low fuel flow. The other Mn ore showed little methane conversion and poorer conversion of the other gases when compared at similar fuel flows. However, the gas composition attained was rather similar if compared for a similar overall gas conversion. Nonetheless, a slightly higher syngas fraction and H_2 to CO ratio in the product stream was obtained with the Mn ore with lower iron content. In all cases the syngas fraction in the product gas increased with temperature and fuel flow. The formation of fines (attrition rate), particle size distribution, and the bulk density of the oxygen carriers were measured to evaluate their mechanical properties during chemical looping of biomass volatiles.

1. Introduction

1.1. Chemical looping combustion and gasification

CO_2 capture and storage (CCS) has been recognized internationally as one of the most important options for climate mitigation [1,2]. Previously, CCS technologies have had a focus on fossil fuels, but it may be even more important to use CCS with bioenergy, so called bio-energy carbon capture and storage, in order to remove CO_2 from the atmosphere [3,4]. Such "negative emissions" will likely be necessary to meet Paris Agreement climate targets [5]. In comparison to other emerging technologies for CO_2 capture, Chemical-looping combustion (CLC) is a potential break-through technology which is unique in the sense that large costs and energy penalties associated with gas separation [6–9] can be avoided. In CLC, gas separation –the capture of CO_2 – is inherent to the process through the transfer of oxygen from air to fuel using solid metal oxides, and thus fuel and air are never mixed. The CLC system is composed of two interconnected fluidized bed reactors i.e. an air reactor

(AR) and a fuel reactor (FR) where oxygen carriers in the form of metal oxide particles transfer oxygen between the two reactors (see Fig. 1) [8, 45]. In the fuel reactor, a fuel reacts with the oxygen carrier (bed materials in the form of a metal oxide Me_xO_y) and in the air reactor, the oxygen carrier is reoxidized (see Eq. (1)) with air and the air reactor releases oxygen-depleted air.

Chemical-Looping Gasification (CLG) is a gasification technology based on the CLC process where a syngas, mainly CO and H_2, is produced in the fuel reactor. The fuel is pyrolyzed and the remaining char is gasified in the fuel reactor by addition of steam or CO_2 resulting in a gas containing gasification products and volatiles (H_2, CO, CO_2, CH_4, and minor amount of C_2 and C_3 species, tars) as well as solids in the form of char and ash [10]. Biomass volatiles are released upon heating and typically constitute 80 wt% of the original fuel on a dry basis [3]. The oxygen carrier (Me_yO_x) can react with the gases released according to Eq. (2).

$$M_xO_{y-n} + \frac{n}{2}O_2 \longrightarrow M_xO_y \tag{1}$$

$$M_xO_y + volatiles \rightarrow \quad H_2 + CO + CO_2 + \quad CH_4 + H_2O + M_xO_{y-n} \tag{2}$$

In CLC the volatile matter is required to be converted to CO₂ and H₂O to the highest extent possible. But in CLG it is desired that the gaseous species are converted to H₂ and CO in the fuel reactor. CLG is similar to normal indirect gasification, but at optimal conditions there will be no combustion of fuel in the air reactor and therefore a high degree of carbon capture can be achieved. In CLG, the gasification atmosphere is more oxidizing compared to indirect gasification and the use of metal oxide particles may also provide catalytic sites for hydrocarbon reactions, thus enhancing syngas production and suppressing tar formation [11–13]. In addition, as no combustion will take place in the air reactor, corrosion on heat transfer surfaces can be limited, which could be highly advantageous [12]. A significant fraction of the carbon should be converted to CO₂ in the fuel reactor, in order to achieve autothermal operation. This is an important difference compared to indirect gasification, where a large fraction of this CO₂ is generated in the air or combustion reactor, thus being diluted with nitrogen. The principles of CLC and CLG are illustrated in Fig. 1. A related process is chemical looping reforming (CLR), where the purpose is to convert a hydrocarbon containing gaseous fuel, e.g. natural gas, to syngas [14].

1.2. Oxygen carriers

Oxygen carriers must fulfil several requirements to be suitable for the chemical looping process. For instance, they must show high reactivity in both the reduction and oxidation stages, high mechanical strength, low agglomeration tendency, long lifetime, and preferably low cost [15]. In addition, these materials should be environmentally benign [16, 17]. In the case of CLG and CLR, oxygen carriers are expected to display high conversion rate of hydrocarbons such as CH₄, C₂ and C₃ species and selectivity towards CO and H₂ [15]. Moreover, several investigations have explored the performance of oxygen carriers in continuous CLC operation using solid fuels, including biomass [7,8,18,19].

Numerous oxygen carriers based on Cu, Co, Mn, Fe, and Ni have been studied for chemical looping process during the last 20 years [20,21,46]. In this regard, natural ores of manganese and iron are at the center of attention for chemical-looping technology owing to their low cost and proven reactivity [3,6]. Mn-based oxygen carriers, including Mn ores, belong to the group of materials with gas phase oxygen release potential, i.e. oxygen uncoupling which is beneficial for oxidizing the gaseous fuels, e.g. biomass volatiles [22–26]. The potential oxygen release properties of Mn-based oxygen carriers are attributed to Mn₂O₃/Mn₃O₄ phases but as Mn₂O₃ is not stable at relevant temperatures, the main phase transition is expected to be Mn₃O₄/MnO which does not involve O₂ release [27]. Nevertheless, it has been shown that presence of Fe, and its ratio to Mn in Mn-based oxygen carriers greatly promote the oxygen release properties which is relevant to Mn ores [28]. Mn-Fe based oxygen carriers supported on geopolymers, have been studied with respect to reactivity in gas conversion, tar decomposition, and oxygen release [29,30]. Experimental investigation of many manganese ores has revealed that almost all of them showed a level of oxygen release in gas phase [31,32]. Also the presence of silica may provide oxygen release as reported by Shulman et al. [33].

Mn ores have been studied in batch fluidized bed setups and in continuous operation with different fuels in 0.3–100 kW CLC units and showed good reactivity in methane and syngas conversion [3,34,35]. In the case of CLG of biomass there are reported works where Mn ores were used as oxygen carriers. However, there is limited research related to the conversion of the volatile matter as the major constituent of biomass fuel. For instance, Moldenhauer et al. [3] tested several manganese ores in a 0.3 kW unit and used synthetic biomass volatiles as fuel for CLC. CO₂ yield of 98% was reported together with almost full conversion of C₂ and C₃ species. The reactivity toward methane was improved at higher temperature. With respect to CLR, the majority of the reported literature is based on methane reforming for hydrogen and syngas production focusing on Fe, Cu, and Ni based oxygen carriers in fixed bed reactor systems [15,36].
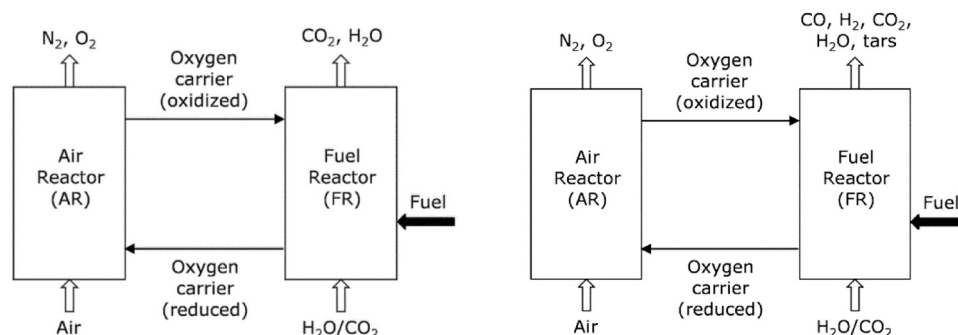

Fig. 1. Chemical-looping combustion (left) and chemical-looping gasification (right) principles [6].

1.3. Scope of the paper

In this work, the two manganese ores with different iron content have been investigated in a chemical-looping reactor system. The aim of the study is to investigate the performance of the two Mn ores as oxygen carrier for chemical looping combustion and partial combustion, the latter in order to assess their suitability for chemical-looping gasification. A number of studies have indicated the that Mn ores could be suitable oxygen carriers for chemical looping but their behavior under conditions under conditions relevant for chemical-looping gasification have received little attention so far. Moreover, as the composition of Mn ores differs, it has an interest to compare the behavior of different ores. As fuel, this study uses a gas mixture representing the gas which is released from biomass during gasification.

2. Materials and methods

2.1. Oxygen carrier materials

Two manganese ores were used in this study as oxygen carriers for chemical looping gasification i.e. Sibelco Calcined (SC) and Elwaleed Grade B (EB). The first ore was supplied by Sibelco Nordic AB and is of unknown origin, whereas the second originates from Egypt. The main phases present in the tested manganese ores are Mn_3O_4, Fe_2O_3, and SiO_2. It should be noted that EB possesses a higher iron oxide content (23 wt %) compared to SC (7.4 wt%) which is the main difference between the two oxygen carriers tested in this work. The Mn ores were calcined in air at 950 °C for 24 h to ensure full oxidation of the oxygen carriers. The calcined particles were sieved to obtain a size range of 0–212 μm, to be loaded into the 300 W reactor. Particles calcined in air are denoted "fresh" and particles recovered from the reactor after the experiments (oxidized) are denoted "used".

2.2. Characterization of oxygen carriers

Elemental composition and oxide phases of the oxygen carriers were analyzed using ICP-SFMS (Inductively Coupled Plasma – Sector Field Mass Spectrometry) and a X-Ray power diffraction (Siemens 5000 X-Ray diffractometer), respectively. Bulk density of the fresh (calcined) and used particles was measured according to ISO standard 3923-1 by pouring the material into a cylinder of defined volume (10.092 cm^3)

through a funnel and weighing the mass of particles in the cylinder. The particles were homogenized using a particle distributor and the density measurement was repeated 5 times for each sample (fresh or used). As an indicator of the attrition and agglomeration of the particles during the operation, the particle size distribution of the fresh and used particles was obtained by sieving the particles in the range of 45, 90, 125, 150, 180, and 212 μm. Particles smaller than 45 μm are too small for use in a fluidized bed combustion process and are denoted "fines" in this work. The outlet streams of the AR and FR were filtered to trap and collect the fines that were formed during the operations. Given the total hours of operation, the attrition rate of the oxygen carriers was calculated as the rate of the weight loss of in the form of fines per hour, divided by the initial weight of the particles loaded into the reactor.

2.3. 300 W chemical looping fluidized bed reactor

Experiments were conducted in a 300 W reactor system where oxygen carriers can be investigated under continuous circulation of particles and continuous fuel feed. The schematic illustration of the 300 W chemical-looping reactor used in this work is shown in Fig. 2.

The reactor system is made of 253MA high temperature chromium-nickel stainless steel alloy suitable for the severe conditions. Previous experience with this material in CLC pilots indicates that the material has a lifetime at least well exceeding 1000 h of operation. The reactor is 300 mm high with a cross-section of 25 mm × 25 mm for the fuel reactor (FR) and 25 mm × 42 mm for the air reactor (AR). The AR has a narrower riser of 25 mm × 25 mm and is operated at a gas velocity sufficient to transport the particles upwards, thus accomplishing the circulation of bed material. There is a gap between the two reactors to minimize the risk of leakage between them. There are two wind boxes located in the bottom of each reactor to let the gas into each reactor via porous quartz plates which act as gas distributors. There is a top part over each reactor where the cross section of both reactors widens, the gas velocity decreases and elutriated particles fall back into the reactors. On the AR side, a part of the particles fall into a loop seal that connects the AR to FR. On the FR side, particles drop directly back into the FR. The loop seals are fluidized with inert gas. From the bottom of the FR, particles pass through the lower loop-seal and return to the AR where the cycle starts over, and the loop is complete. The exit pipe of the FR is connected to a water seal with a column height of less than 2 cm to keep a higher pressure of 0.1–0.2 kPa, in the FR compared to AR in order to
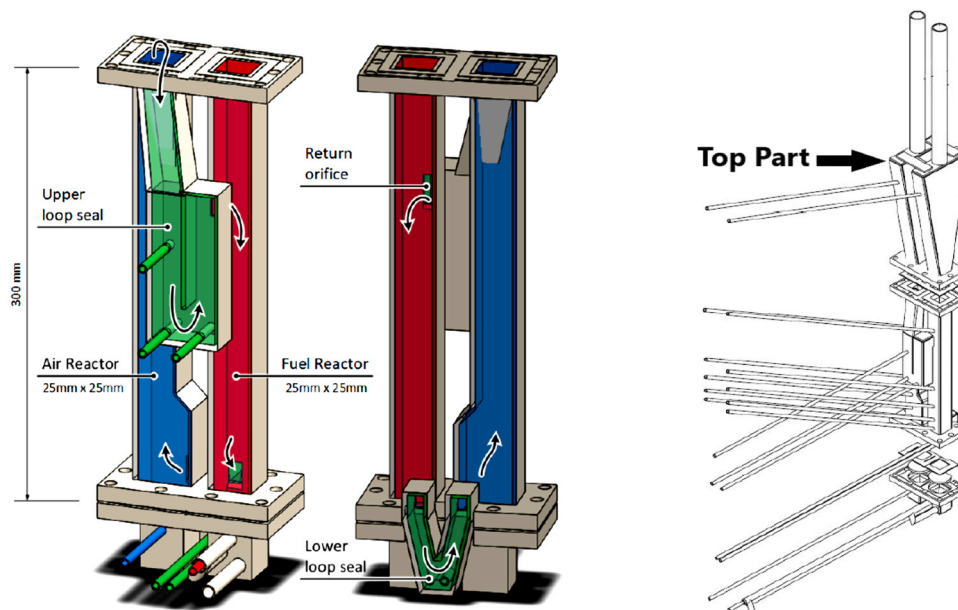

Fig. 2. 300 W reactor (left) and its technical drawing (right) [37].

reduce gas leakage from AR to FR. The bed temperatures of AR and FR are measured by means of K-type thermocouples. The 300 W reactor is located inside an electrical furnace that controls the temperature. The fluidization and the circulation are monitored via pressure difference measurement at different locations.

2.4. Experimental procedure

The reactor was fed with around 0.4 kg of oxygen carriers. Prior to the experiments, the oxygen carriers were activated with syngas (50% hydrogen in CO) at 900 °C for 2 h. Oxygen carriers were circulating during the activation and the AR air flow rate was 8 Lmin^{-1}. In this work a synthesized gas mixture (BMV) was used to simulate biomass volatiles for the experiments in the 300 W reactor. This composition was chosen to represent the gases generated via devolatilization of wood-based biofuels. This composition resembles the gas generated during operation of the Chalmers 2 MW gasifier, albeit excluding tars and higher hydrocarbons [38]. The lower heating value of the gas composition used is 20.2 MJm^{-3}. The composition of BMV fuel is given in Table 1.

Five BMV flow rates were selected in order to investigate methane, CO and H$_2$ conversion, the attrition and circulation behavior of the particles. The BMV flow rates are 0.6, 0.9, 1.2, 2, and 3 Lmin^{-1} corresponding to an overall air-fuel equivalence ratio, λ, of 3.2–0.6. The air flow rates in the AR were 8 and 9 Lmin^{-1} for SC and EB, respectively, which gives a riser velocity of 0.9–1.0 ms^{-1}. The circulation rate of the particles between AR and FR varied between 0.8 and 1.7 gs^{-1} for SC and 2.6–3.5 gs^{-1} for EB depending on the temperature and the fuel flow. In the case of EB the air flow in AR was set to 9 Lmin^{-1} to have enough circulation and avoid defluidization in the fuel reactor which can occur when the oxygen carrier is highly reduced. Experiments were carried out at a temperature of 850 and 900 °C in the FR. The experimental procedure is given in Table 2. The reactor was cooled down to room temperature in air at the end of each experiment. The composition of the gases arising from the FR was analyzed using an Agilent Micro GC CP-4900 and online gas analyzers (SICK Extractive Gas Analyzer SIDOR).

The large surplus of oxygen in the air reactor, as indicated by the high values of λ, is not necessarily available in the fuel reactor, where the availability of oxygen depends on the reactivity of the oxygen carrier as well as bed mass and circulation. The latter two were both kept constant during the tests, while fuel flow was varied. To facilitate the comparison of the experimental results, an effective air ratio is used in the evaluation below.

2.5. Data evaluation

In this work, the effect of temperature and fuel flow rate on syngas fraction and the fraction of methane in the flue gas from the FR are given based on Effective Air Ratio (λ$_{eff}$) which is defined as the ratio between the oxygen which is transferred from AR to the gas phase in FR by the oxygen carriers and the oxygen needed for full combustion of the fuel (stoichiometric oxygen).

$$\lambda_{eff} = \frac{oxygen\ transferred\ from\ AR\ to\ FR}{oxygen\ needed\ for\ full\ combustion} \tag{3}$$

λ$_{eff}$ allows evaluating the data on a normalized basis. The Effective

Table 1
The composition of the synthetic biomass volatiles fuel (BMV).

Component	Fraction (vol%)	Carbon fraction (atomic %)
CO	43.0	55.1
H$_2$	30.0	–
CH$_4$	20.0	25.6
C$_2$H$_4$	6.0	15.4
C$_3$H$_6$	1.0	3.8
Total	100.0	99.9

Air Ratio is also equal to the gas conversion efficiency (η$_{gas}$) in the FR [39]:

$$\lambda_{eff} = \eta_{gas} = 1 - \Omega_{OD} \tag{4}$$

where Ω$_{OD}$ is the oxygen demand:

$$\Omega_{OD} = \frac{0.5x_{CO} + 2x_{CH_4} + 0.5x_{H_2} + 3x_{C_2H_4} + 4.5x_{C_3H_6}}{\Phi_0(x_{CO} + x_{CH_4} + 2x_{C_2H_4} + 3x_{C_3H_6})} \tag{5}$$

where x$_i$ is the volume fraction of the gas i and Φ_0 is the molar ratio [n$_{O2}$ required for combustion/kg fuel]/[n$_C$/kg fuel] [35]:

$$\Phi_0 = \frac{0.5y_{CO} + 2y_{CH_4} + 0.5y_{H_2} + 3y_{C_2H_4} + 4.5y_{C_3H_6}}{y_{CO} + y_{CH_4} + 2y_{C_2H_4} + 3y_{C_3H_6}} \tag{6}$$

where y is the carbon content of each species in the fuel based on the composition given in Table 2. For the fuel used in this work, Φ_0 is equal to 1.27.

λ$_{eff}$ depends mainly on the fuel flow rate, temperature, and nature of the oxygen carries as the oxygen uptake and reactivity varies for the different materials. Lower fuel flow gives higher gas conversion, thus higher effective air ratio.

The syngas fraction in the product gas (f$_{syngas}$), is defined as the fraction of H$_2$ and CO in the gas leaving the reactor, on a dry basis.

$$f_{syngas} = \frac{x_{CO} + x_{H_2}}{x_{CO} + x_{CO_2} + x_{CH_4} + x_{H_2} + x_{C_2H_4} + x_{C_3H_6}} \tag{7}$$

The carbon fraction, f$_i$, is the molar ratio of species i normalized to total carbon and is defined as follows:

$$f_i = \frac{x_i}{x_{CO} + x_{CO_2} + x_{CH_4} + 2x_{C_2H_4} + 3x_{C_3H_6}} \tag{8}$$

where i is any of H$_2$, CO, CO$_2$, CH$_4$, or C$_n$H$_{2n}$ and x is the volumetric ratio and the denominator represents the total carbon in the outlet stream. To compare the conversion or production of different species with respect to incoming fuel, the ratio between the carbon fraction in the inlet (with the superscript in) and outlet stream (with the superscript out) of the fuel reactor is defined as follows:

$$FR\ conversion\ ratio = \varphi_i = \frac{f_i^{out}}{f_i^{in}} \tag{9}$$

For the synthetic BMV used in this work f$_i^{in}$ of CO, H$_2$, CH$_4$, and C$_n$H$_{2n}$ are 0.55, 0.38. 0.26, and 0.09, respectively, given that the total carbon content (mol.%) is 0.78.

The syngas to hydrocarbon ratio is defined as follows:

$$syngas\ to\ hydrocarbon\ ratio = \frac{0.5x_{CO} + 0.5x_{H_2}}{2x_{CH_4} + 3x_{C_2H_4} + 4.5x_{C_3H_6}} \tag{10}$$

3. Results and discussion

The gas conversion, or effective air ratio, is shown as function of temperature and fuel flow in Table 3. As can be seen, full gas conversion is reached for EB at 900 °C and the lowest fuel flow, whereas the conversion of SC was quite low even for the lowest fuel flow, and at all conditions SC showed considerably lower conversion. Thus, it is clearly established that EB has a much higher gas conversion of the two ores.

As an example, the concentration of dry gases in the outlet of the FR is shown in Fig. 3 for EB at 900 °C using simulated biomass volatiles as fuel. The FR was fluidized with argon before operating with fuel. All the fuel is converted to CO$_2$ at a fuel flow rate of 0.6 Lmin^{-1}. Then, at 0.9 Lmin^{-1} methane and carbon monoxide appear as the fuel flow increases. It is seen that the conversion to CO$_2$ is falls with fuel flow rate while, in particular, unconverted methane rises.

Also shown in Fig. 3 is the concentration of oxygen in the outlet gas of AR, dotted line, which decreases with the fuel flow rate. The outlet

Table 2

Experimental conditions employed during experimental campaigns.

	Purpose	FR fuel flow [Lmin^{-1}]	λ [-]	FR temperature [°C]	AR air flow [Lmin^{-1}]	Run time [hrs]
SC						
Syngas	Activation	1	1.7	900	8	2
BMV	Study	0.6 – 3	2.8 – 0.6	850–900	8	27
EB						
Syngas	Activation	1	1.7	900	8	2
BMV	Study	0.6 – 3	3.1 – 0.6	850 – 900	9	18

Table 3

The effective air ratio or gas conversion, for different fuel flows and temperatures. The corresponding standard deviation of the data presented is below 0.01.

BMV flow (Lmin^{-1})	$\lambda_{eff} = \eta_{gas} = 1 - \Omega_{OD}$			
	T = 850 °C		T = 900 °C	
	SC	EB	SC	EB
0.6	0.52	0.86	0.61	1
0.9	0.51	0.79	0.56	0.87
1.2	0.44	0.71	0.49	0.78
2	0.39	0.57	0.43	0.58
3	–	0.44	0.39	0.49
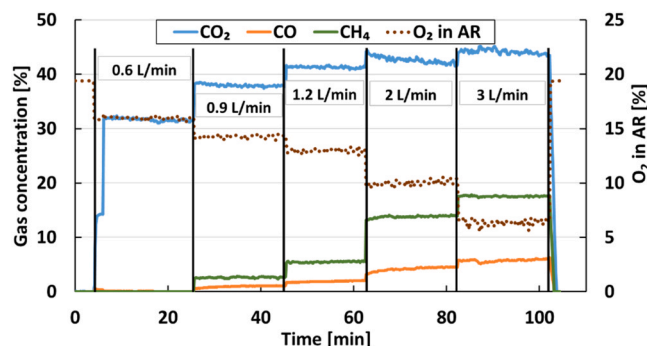
Fig. 3. The concentration of outlet dry gas from the FR when operating with EB at 900 °C. The dotted line shows the oxygen concentration in the outlet of AR.

concentrations from the FR did not sum up to 100% since the loop seals of the 300 W reactor were fluidized by argon that is mixed with the FR and AR outlet streams. After the period of 3 Lmin^{-1} fuel flow, the fuel is stopped and argon is added to the FR. Here, concentrations of measured gases from the FR go to zero and the oxygen concentration in AR returns to its initial concentration.

Table 3 clarified the differences between the two materials, with respect to CLC. In gasification, however, limited oxidation of the fuel is desired in order to minimize energy losses, and therefore it is of interest to compare the conversion of the fuel gases, at similar effective air ratios.

The carbon fraction (f_i) as calculated from Eq. (8), in the outlet gas from the FR gives the first assessment of the experiments with SC and EB and how these particles differ in operation. The carbon fraction of CO, CO_2, and CH_4 in the exhaust gas from FR for both particles is shown in Fig. 4 as a function of λ_{eff}. In the case of EB most of the carbon was converted to CO_2 and the rest of the gas mainly consisted of CH_4.

The main feature in Fig. 4 is the wider range of λ_{eff} in the case of EB as compared to SC, a consequence of its ability to reach high gas conversion.

The fraction of methane (f_{CH_4}) in the FR outlet is an indicator of the reactivity of oxygen carriers toward methane. In the case of EB at 900 °C and 0.6 Lmin^{-1} of BMV, 100% methane conversion was reached. High methane conversion to CO_2 and H_2O is desired in CLC. It is also highly beneficial in CLG, as high methane content may not be beneficial for further downstream processes, such as Fischer-Tropsch synthesis. However, partial methane reforming to syngas is preferred rather than full oxidation in the case of CLG. Mn-based oxygen carriers are generally less reactive toward CH_4 as compared to H_2 and CO [3,27,31] which could result in rapid and selective conversion of CO compared to CH_4.

The conversion ratio, Eq. (9), gives a clearer idea of the extent of the conversion of the key components, i.e. CO, H_2, CH_4, and C_2H_4. No C_3H_6 was detected by the GC. The overlapping results in Fig. 4 and Fig. 5 indicate that approximately similar gas conversions were reached at similar values of λ_{eff} for SC and EB. For example, at λ_{eff} below 0.5 little methane was converted (Fig. 5c) by either of the oxygen carriers. In contrast, the conversion of hydrogen and CO is still high at lowest value of λ_{eff} reached.

3.1. Oxygen release properties

Some oxygen carriers have the ability to release gas-phase oxygen in a reducing or inert environment [32]. In the case of manganese oxides, Mn_2O_3 releases oxygen when it decomposes to Mn_3O_4 [32,40]. However, re-oxidation of Mn_3O_4 back to Mn_2O_3 is thermodynamically not possible at the operating conditions in the AR, although some oxygen release properties have been reported before [41]. SC and EB oxygen
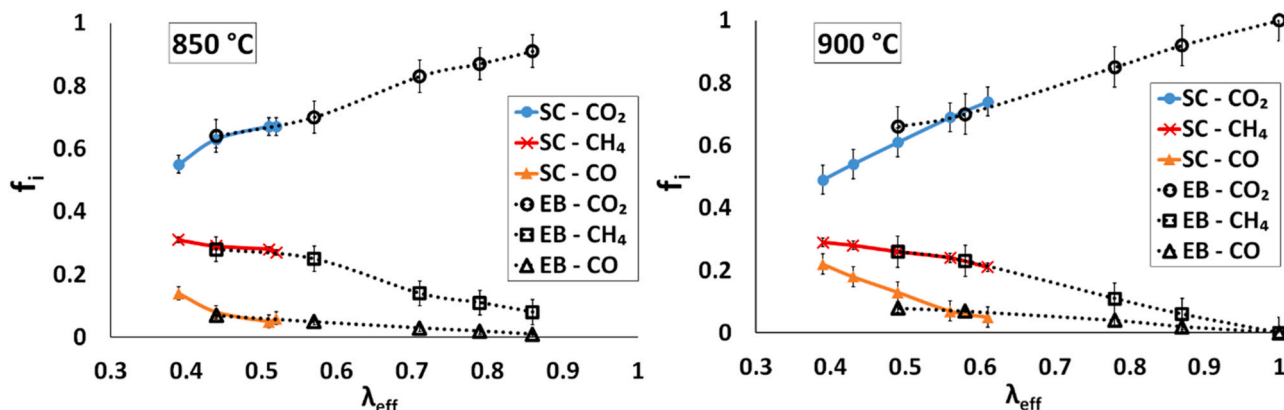
Fig. 4. Fraction of CO, CO_2, and CH_4 in the FR outlet.
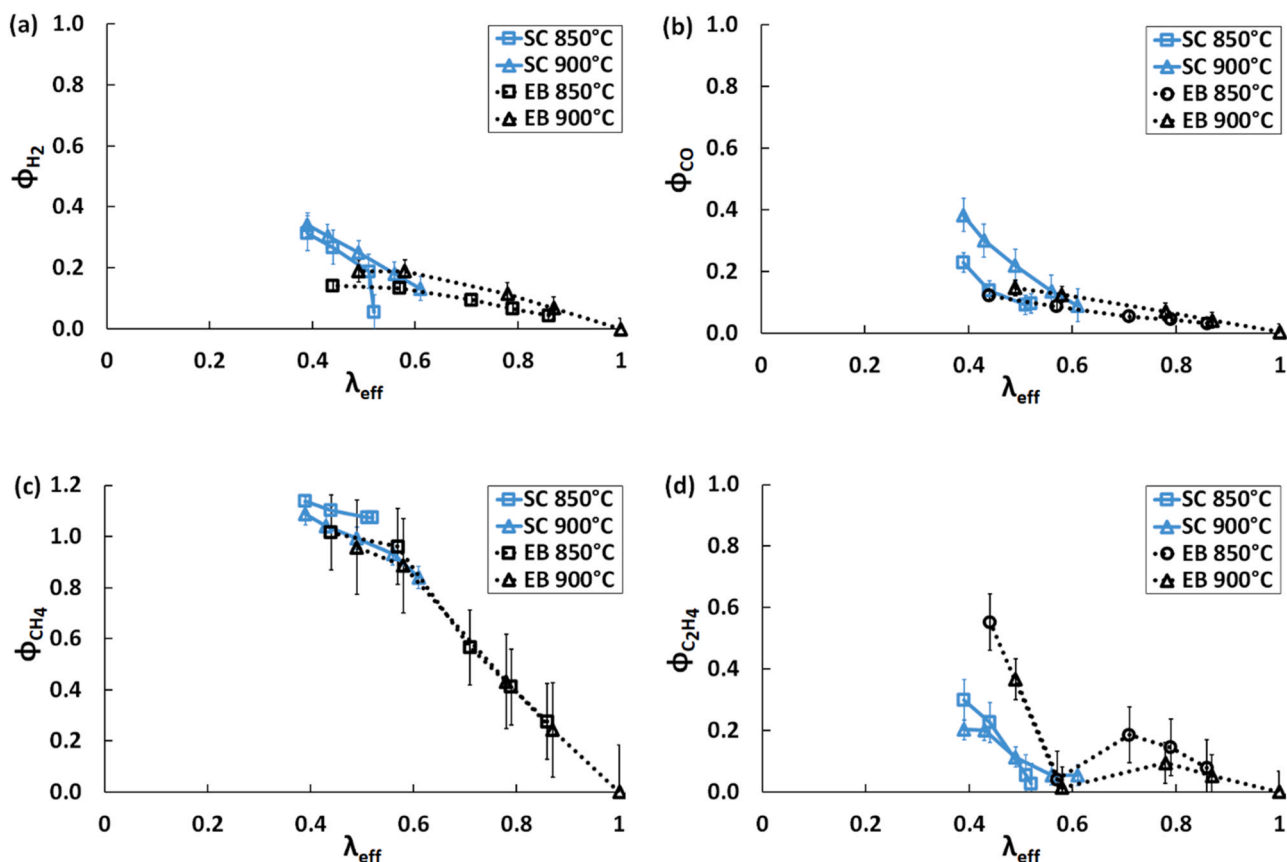
Fig. 5. Conversion ratio of the key species vs λ_{eff}.

carriers have been tested by Sundqvist et al. [27,32] in batch fluidized bed reactors. Both oxygen carriers released some oxygen, but CH_4 and CO conversion were notably higher in the case of EB. In this work, SC and EB showed stable oxygen release of 0.4% and 4.0% volume, respectively, when FR is fluidized with 1 $Lmin^{-1}$ of argon at 900 °C. At 850 °C, the concentrations were lower, 0.1% and 2%.

According to Azimi et al. [42,43], the oxygen release properties can be ascribed to Mn-Fe-O phases which contribute to very high and rapid oxygen release. The presence of Fe in the Mn ores, especially in EB, can explain the observed oxygen release and agrees with previously reported findings. Such release is favorable for CLC, but not necessarily for CLG.

3.2. Syngas fraction

Important for the CLG process is the syngas fraction in the outlet of the FR. As shown in Fig. 6, the syngas fraction in the case of SC seems somewhat higher than that obtained with EB but the difference is small for the similar values of λ_{eff}. The fraction of syngas, and syngas to hydrocarbon ratio of the incoming fuel (synthetic BMV, Table 1) are given at $\lambda_{eff} = 0$ in Fig. 6. Thus, the curve in Fig. 6 should reach the values for the incoming fuel as λ_{eff} approaches zero.

The key difference between SC and EB is that EB is able to convert CH_4 at low fuel flow, whereas SC is essentially unable to do so. But when compared at similar effective air ratio, which is relevant for gasification, the difference between the materials is rather small.
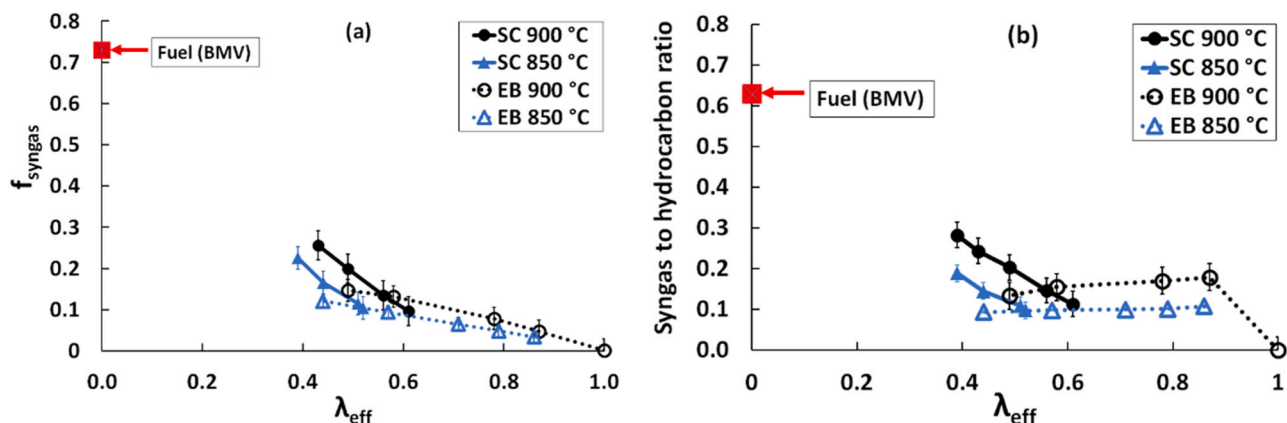

Fig. 6. Syngas fraction (a) and syngas to hydrocarbon ratio (b).

3.3. Analysis of particles

3.3.1. Attrition and particle size distribution (PSD)

The lifetime of the particles is one of the main parameters for selection of proper oxygen carrier for the chemical looping process. At CLC conditions, particles are exposed to high-velocity impacts and thermochemical stress. Thus, oxygen carrier particles undergo mechanical degradation in a circulating fluidized bed reactor and they eventually turn to dust or fines and may leave the reactor together with the gas flow [35]. Therefore, it is crucial to monitor and measure the attrition behavior of the particles in realistic conditions i.e. operation with fuel at high temperature. Density of the oxygen carriers before and after the experiments is an indicator of possible changes in the physical properties of the particles. Density and attrition rates of the fresh and used materials are shown in Table 4. SC particles are initially denser than EB, but show more decrease in density. The total operation corresponds to the operating time with fluidization and circulation at high temperature (850–900 °C) in reducing environment (inert or fuel).

For the sieved and homogenized batch of fresh particles, SC contains bigger particles than EB, as seen in Fig. 7.

Most of the used particles are in the size range of 90–210 μm for SC oxygen carrier while this range shifts to around 60–180 μm in the case of EB. As seen in Table 4, the attrition rate of EB particles is higher than SC.

Although the bulk density of both SC and EB has decreased after the experiments, in the case of SC the density change is remarkable. According to Fig. 7, the PSD of the used SC shows a shift towards larger particles which could be explained by decrease in bulk density, see Table 4. The PSD for used EB particles indicates a formation of both smaller and larger particles, i.e. smaller than 90 μm and bigger than 210 μm. In this case, particle agglomeration and formation of fines both occurred. This was evident as small lumps of particles were observed after the experiments with EB.

SEM images of the fresh and used particles indicate that fresh particles are homogeneous with little cracks and visible pores, Fig. 8a and c. This is in contrast to used EB particles, Fig. 8d, that have more cracks and pores compared to used SC particles, Fig. 8) which may have contributed to higher fines formation of EB particles, Table 4. The SEM images were taken from the particles smaller than 212 μm.

The attrition data corresponds to a lifetime of 200 and 330 h for EB and SC. Compared to the attrition rates reported by Moldenhauer et al. [3] where other Mn ores were tested at conditions similar to this work, SC and EB are in the middle of the range. As reported by Moldenhauer et al. [3], Guizhou with attrition rate of 0.05 w%hr^{-1} is highly resistant to attrition. On the contrary, Tshipi Mn ore was very prone to dusting with an attrition rate of 1.1 w%hr^{-1}. SC has been reported previously to have a low attrition rate compared to other Mn or Fe ores, with an estimated lifetime of 750 h in a 10 kW pilot and 700 h in a 10 kW pilot [44]. The higher attrition rate found in this paper is likely associated with the attrition being higher initially.

3.3.2. Phase composition

X-Ray powder diffraction of as-received (not calcined), used, and reduced particles were done to investigate the phase changes during the experiments. Used samples were fully oxidized by air in the reactor after the experiments. Reduced samples were prepared using a special quartz batch reactor setup where a simple and single reduction step was carried out by purging 800 ml of CO into the reactor at 900 °C and cooling down to the room temperature in nitrogen. For this purpose, used particles from the FR after the experiments were employed. An explanation of the batch reactor setup can be found in several previous works [26,27,32]. The phases detected in the XRD diffractograms of as-received (not calcined), used, and reduced oxygen carriers are given in Table 5.

The identified phases are similar to what was reported in the literature for similar cases [27,32]. MnO_2 is present in EB fresh samples, which was reduced to Mn_2O_3 and then Mn_3O_4 upon calcination. Because thermodynamic restraints prevent the oxidization of manganese oxides back to MnO_2 or Mn_2O_3, the expected redox cycle of manganese oxide involves $Mn_3O_4 \leftrightarrow MnO$, which does not release oxygen. For SC, the XRD shows the presence of $(Mn,Fe)_2O_3$ and $(Mn,Fe)_3O_4$ in used and reduced samples, respectively, which is known to release oxygen. For EB $(Mn, Fe)_3O_4$ is seen and no Fe_2O_3 or Mn_3O_4 was distinctly detected in the fully oxidized sample which could possibly be because of difficulties in distinguishing between phases. Thus, the higher stable oxygen release of EB can be a result of higher iron content [42].

4. Conclusions

Two different manganese ores, i.e. Sibelco Calcined (SC) and Elwaleed B (EB), were investigated in a chemical looping reactor system with simulated biomass volatiles. EB was found to be more reactive than SC, with the latter showing low methane conversion even at low fuel flows. The highlights of the results can be listed as below:

   I. Almost the same syngas fractions were reached in the case of SC and EB for the same effective air ratio, i.e. for the same overall gas conversion.
  II. Methane conversion was very low in the case of SC during the whole range of operation whereas in the case of EB full conversion was observed at low fuel flow rate and 900 °C.
 III. For an effective air ratio below 0.5, where CLG would be operated, essentially no CH_4 conversion was seen for either of the two materials. This is a clear disadvantage if the desired product is syngas.
 IV. C_3 species were completely converted in all operating conditions.
  V. High fuel flow rate and high temperature favored syngas yield in the outlet stream of the FR.

Moreover, fines formation and particle size distribution (PSD) measurements showed that SC had better physical properties and a lower attrition rate than EB. Furthermore, EB showed much higher oxygen release, which was attributed to the higher Fe content, in accordance with previous findings reported in the literature. It was concluded that under the operating conditions used in this work, SC is likely a better oxygen carrier for CLG because of better mechanical properties of the particles. On the other hand, the much higher gas conversion of EB indicates that this material should be the best of the two for CLC.

CRediT authorship contribution statement

Ali Hedayati: Data curation, Formal analysis, Methodology, Writing - original draft, Writing - review & editing. **Amir H. Soleimanisalim**: Data curation, Writing - review & editing. **Carl Johan Linderholm**: Funding acquisition, Project administration, Supervision, Writing - review & editing. **Tobias Mattisson**: Funding acquisition, Methodology, Project administration, Supervision, Validation, Writing - review & editing. **Anders Lyngfelt**: Investigation, Methodology, Resources, Validation, Writing - review & editing.

Declaration of Competing Interest

The authors declare that they have no known competing financial interests or personal relationships that could have appeared to influence
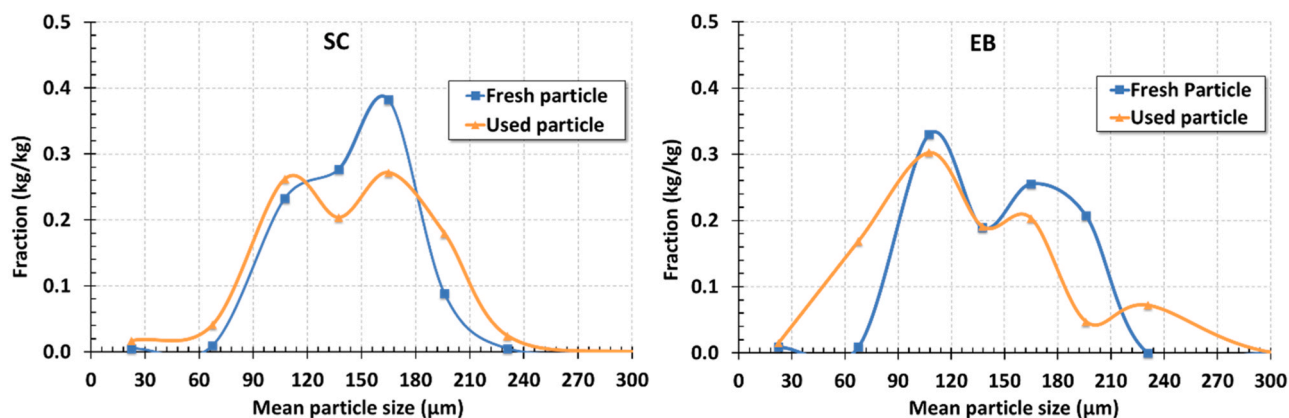
Table 4
Bulk density and attrition rate of the fresh and used particles.

Particle	Bulk Density-Fresh [gcm^{-3}]	Bulk Density-Used [gcm^{-3}]	Attrition [w%hr^{-1}]	Total operation [hrs]	Operation with fuel [hrs]
SC	1.9	1.4	0.3	27	20
EB	1.5	1.3	0.5	18	14

Fig. 7. Particle size distribution (PSD) of fresh and used (fully oxidized) oxygen carriers.
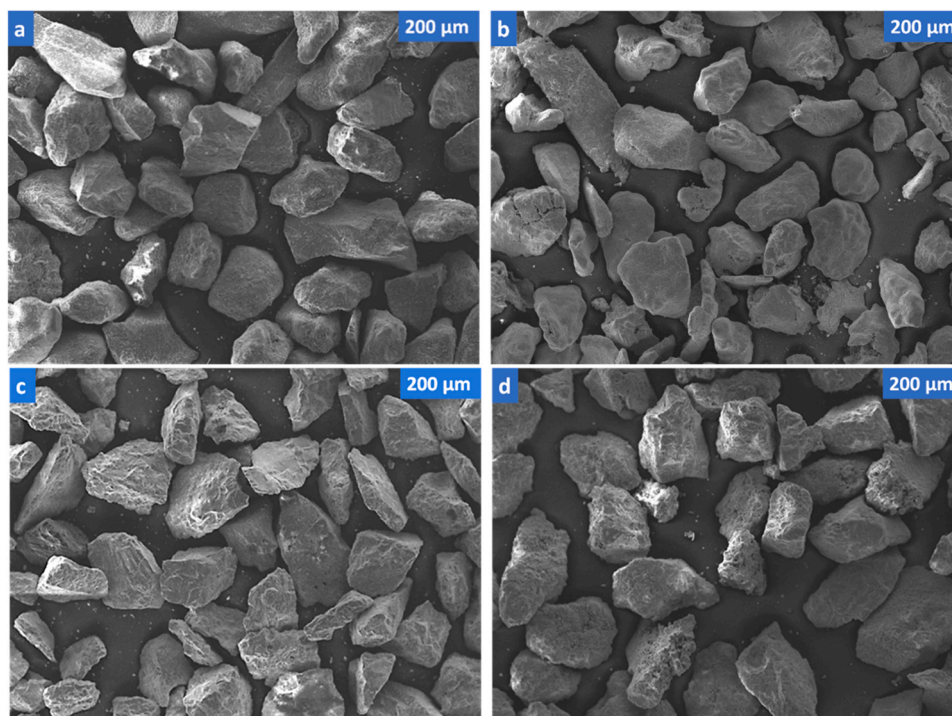

Fig. 8. SEM images of SC fresh (a), SC used (b), EB fresh (c), and EB used (d).

Table 5

Characterization of Mn ores with XRD with main crystalline phases identified in as-received (not calcined), used, and reduced samples used in this work.

	Fresh (As received)	Used (fully oxidized)	Reduced (2 wt% conversion)
SC	MnO, Mn_3O_4, $(Mn, Fe)_2O_3$	Mn_3O_4, $(Mn,Fe)_2O_3$	MnO, $(Mn,Fe)_3O_4$
EB	MnO_2, $(Mn,Fe)_2O_3$, SiO_2	Mn_3O_4, $(Mn,Fe_3)O_4$, SiO_2	MnO, $(Mn,Fe)_3O_4$, SiO_2

the work reported in this paper.

References

[1] IPCC, 2014. Climate Change 2014: Synthesis Report. Contribution of Working Groups I, II and III to the Fifth Assessment Report of the Intergovernmental Panel on Climate Change, Geneva, Switzerland, (2014).

[2] A.H. Soleimanisalim, M.H. Sedghkerdar, D. Karami, N. Mahinpey, Effects of second metal oxides on zirconia-stabilized Ca-based sorbent for sorption/catalyst integrated gasification, J. Environ. Chem. Eng. 5 (2017) 1281–1288, https://doi.org/10.1016/j.jece.2017.01.047.

[3] P. Moldenhauer, S. Sundqvist, T. Mattisson, C. Linderholm, Chemical-looping combustion of synthetic biomass-volatiles with manganese-ore oxygen carriers, Int. J. Greenh. Gas Control 71 (2018) 239–252, https://doi.org/10.1016/J.IJGGC.2018.02.021.

[4] T. Mendiara, F. García-Labiano, A. Abad, P. Gayán, L.F. de Diego, M.T. Izquierdo, J. Adánez, Negative CO_2 emissions through the use of biofuels in chemical looping technology: a review, Appl. Energy 232 (2018) 657–684, https://doi.org/10.1016/J.APENERGY.2018.09.201.

[5] United Nations, The Paris Agreement, (2015). ⟨https://unfccc.int/process-and-meetings/the-paris-agreement/the-paris-agreement⟩.

[6] P. Moldenhauer, C. Linderholm, M. Rydén, A. Lyngfelt, Avoiding CO_2 capture effort and cost for negative CO_2 emissions using industrial waste in chemical-looping combustion/gasification of biomass, Mitig. Adapt. Strateg. Glob. Change 25 (2019) 1–24, https://doi.org/10.1007/s11027-019-9843-2.

[7] J. Adánez, A. Abad, T. Mendiara, P. Gayán, L.F. de Diego, F. García-Labiano, Chemical looping combustion of solid fuels, Prog. Energy Combust. Sci. 65 (2018) 6–66, https://doi.org/10.1016/J.PECS.2017.07.005.

[8] A. Lyngfelt, Chemical-looping combustion of solid fuels – status of development, Appl. Energy 113 (2014) 1869–1873, https://doi.org/10.1016/J.APENERGY.2013.05.043.

[9] A. Lyngfelt, B. Leckner, A 1000 MWth boiler for chemical-looping combustion of solid fuels – discussion of design and costs, Appl. Energy 157 (2015) 475–487, https://doi.org/10.1016/J.APENERGY.2015.04.057.

[10] D. Neves, A. Matos, L. Tarelho, H. Thunman, A. Larsson, M. Seemann, Volatile gases from biomass pyrolysis under conditions relevant for fluidized bed gasifiers, J. Anal. Appl. Pyrolysis 127 (2017) 57–67, https://doi.org/10.1016/j.jaap.2017.09.002.

[11] A. Kostyniuk, M. Grilc, B. Likozar, Catalytic cracking of biomass-derived hydrocarbon tars or model compounds to form biobased benzene, toluene, and xylene isomer mixtures, Ind. Eng. Chem. Res. 58 (2019) 7690–7705, https://doi.org/10.1021/acs.iecr.9b01219.

[12] T. Mattison, F. Hildor, Y. Li, C. Linderholm, Negative emissions of carbon dioxide through chemical-looping combustion (CLC) and gasification (CLG) using oxygen carriers based on manganese and iron, Mitig. Adapt. Strateg. Glob. Change 25 (2019) 497–517, https://doi.org/10.1007/s11027-019-09860-x.

[13] M. Keller, H. Leion, T. Mattisson, H. Thunman, Investigation of natural and synthetic bed materials for their utilization in chemical looping reforming for tar elimination in biomass-derived gasification gas, Energy Fuels 28 (2014) 3833–3840, https://doi.org/10.1021/ef500369c.

[14] S.G. Nadgouda, M. Guo, A. Tong, L.S. Fan, High purity syngas and hydrogen coproduction using copper-iron oxygen carriers in chemical looping reforming process, Appl. Energy 235 (2019) 1415–1426, https://doi.org/10.1016/j.apenergy.2018.11.051.

[15] J. Adanez, A. Abad, F. Garcia-Labiano, P. Gayan, L.F. De Diego, Progress in chemical-looping combustion and reforming technologies, Prog. Energy Combust. Sci. 38 (2012) 215–282, https://doi.org/10.1016/j.pecs.2011.09.001.

[16] B.L. Salvi, S. Jindal, Recent developments and challenges ahead in carbon capture and sequestration technologies, SN Appl. Sci. 1 (2019) 885, https://doi.org/10.1007/s42452-019-0909-2.

[17] L. Liu, Z. Li, L. Wang, Z. Zhao, Y. Li, N. Cai, MgO-kaolin-supported manganese ores as oxygen carriers for chemical looping combustion looping combustion, (2019). doi:10.1021/acs.iecr.9b05267.

[18] A. Lyngfelt, C. Linderholm, Chemical-looping combustion of solid fuels – status and recent progress, Energy Procedia 114 (2017) 371–386, https://doi.org/10.1016/J.EGYPRO.2017.03.1179.

[19] I. Adánez-Rubio, A. Abad, P. Gayán, L.F. de Diego, F. García-Labiano, J. Adánez, Biomass combustion with CO$_2$ capture by chemical looping with oxygen uncoupling (CLOU), Fuel Process. Technol. 124 (2014) 104–114, https://doi.org/10.1016/J.FUPROC.2014.02.019.

[20] A. Lyngfelt, A. Brink, Ø. Langørgen, T. Mattisson, M. Rydén, C. Linderholm, 11,000 h of chemical-looping combustion operation—where are we and where do we want to go? Int. J. Greenh. Gas Control 88 (2019) 38–56, https://doi.org/10.1016/j.ijggc.2019.05.023.

[21] J.C. Abanades, B. Arias, A. Lyngfelt, T. Mattisson, D.E. Wiley, H. Li, M.T. Ho, E. Mangano, S. Brandani, Emerging CO$_2$ capture systems, Int. J. Greenh. Gas Control 40 (2015) 126–166, https://doi.org/10.1016/J.IJGGC.2015.04.018.

[22] D. Mei, T. Mendiara, A. Abad, L.F. De Diego, F. García-Labiano, P. Gayán, J. Adánez, H. Zhao, Evaluation of manganese minerals for chemical looping combustion, Energy Fuels 29 (2015) 6605–6615, https://doi.org/10.1021/acs.energyfuels.5b01293.

[23] D. Mei, T. Mendiara, A. Abad, L.F. De Diego, F. García-Labiano, P. Gayán, J. Adánez, H. Zhao, Manganese minerals as oxygen carriers for chemical looping combustion of coal, Ind. Eng. Chem. Res. 55 (2016) 6539–6546, https://doi.org/10.1021/acs.iecr.6b00263.

[24] M. Ryden, M. Kallen, D. Jing, A. Hedayati, T. Mattisson, A. Lyngfelt, (Fe$_{1-x}$Mn$_x$)Ti$_y$O$_3$ based oxygen carriers for chemical-looping combustion and chemical-looping with oxygen uncoupling, Energy Procedia 51 (2014) 85–98, https://doi.org/10.1016/j.egypro.2014.07.010.

[25] M. Arjmand, A. Hedayati, A.-M. Azad, H. Leion, M. Rydén, T. Mattisson, Ca$_x$La$_{1-x}$Mn$_{1-y}$M$_y$O$_{3-\delta}$ (M = Mg, Ti, Fe, or Cu) as oxygen carriers for chemical-looping with oxygen uncoupling (CLOU), Energy Fuels 27 (2013) 4097–4107, https://doi.org/10.1021/ef3020102.

[26] A. Hedayati, A. Azad, M. Ryde, H. Leion, T. Mattisson, Evaluation of novel ceria-supported metal oxides as oxygen carriers for chemical-looping combustion, Ind. Eng. Chem. Res. 51 (2012) 12796–12806, dx.doi.org/10.1021/ie300168j |.

[27] S. Sundqvist, N. Khalilian, H. Leion, T. Mattisson, A. Lyngfelt, Manganese ores as oxygen carriers for chemical-looping combustion (CLC) and chemical-looping with oxygen uncoupling (CLOU), J. Environ. Chem. Eng. 5 (2017) 2552–2563, https://doi.org/10.1016/J.JECE.2017.05.007.

[28] G. Azimi, H. Leion, M. Ryde, T. Mattisson, A. Lyngfelt, Investigation of different Mn–Fe oxides as oxygen carrier for chemical-looping with oxygen uncoupling (CLOU), (2013). doi:10.1021/ef301120r.

[29] R. Bendoni, F. Miccio, V. Medri, P. Benito, A. Vaccari, E. Landi, Geopolymer composites for the catalytic cleaning of tar in biomass-derived gas, Renew. Energy 131 (2019) 1107–1116, https://doi.org/10.1016/j.renene.2018.08.067.

[30] F. Miccio, R. Bendoni, A. Piancastelli, V. Medri, E. Landi, Geopolymer composites for chemical looping combustion, Fuel 225 (2018) 436–442, https://doi.org/10.1016/j.fuel.2018.03.153.

[31] S. Sundqvist, M. Arjmand, T. Mattisson, M. Rydén, A. Lyngfelt, Screening of different manganese ores for chemical-looping combustion (CLC) and chemical-looping with oxygen uncoupling (CLOU), Int. J. Greenh. Gas Control 43 (2015) 179–188, https://doi.org/10.1016/J.IJGGC.2015.10.027.

[32] S. Sundqvist, T. Mattisson, H. Leion, A. Lyngfelt, Oxygen release from manganese ores relevant for chemical looping with oxygen uncoupling conditions, Fuel 232 (2018) 693–703, https://doi.org/10.1016/J.FUEL.2018.06.024.

[33] A. Shulman, E. Cleverstam, T. Mattisson, A. Lyngfel, Manganese/iron, manganese/nickel, and manganese/silicon oxides used in chemical-looping with oxygen uncoupling (CLOU) for combustion of methane, Energy Fuels 23 (2009) 5269–5275, https://doi.org/10.1021/ef9005466.

[34] P. Moldenhauer, A. Serrano, F. García-Labiano, L.F. De Diego, M. Biermann, T. Mattisson, A. Lyngfelt, Chemical-looping combustion of kerosene and gaseous fuels with a natural and a manufactured mn-fe-based oxygen carrier, Energy Fuels 32 (2018) 8803–8816, https://doi.org/10.1021/acs.energyfuels.8b01588.

[35] C. Linderholm, M. Schmitz, M. Biermann, M. Hanning, A. Lyngfelt, Chemical-looping combustion of solid fuel in a 100 kW unit using sintered manganese ore as oxygen carrier, Int. J. Greenh. Gas Control 65 (2017) 170–181, https://doi.org/10.1016/j.ijggc.2017.07.017.

[36] D. Li, R. Xu, X. Li, Z. Li, X. Zhu, K. Li, Chemical looping conversion of gaseous and liquid fuels for chemical production: a review, Energy Fuels 34 (2020) 5381–5413, https://doi.org/10.1021/acs.energyfuels.0c01006.

[37] K. Johannsen, Experimental Testing of Oxygen Carriers in a 300 W Chemical-Looping Combustion Reactor, Chalmers University of Technology, 2018.

[38] A. Larsson, M. Israelsson, F. Lind, M. Seemann, H. Thunman, Using ilmenite to reduce the tar yield in a dual fluidized bed gasification system, (2014). doi:10.1021/ef500132p.

[39] C. Linderholm, P. Knutsson, M. Schmitz, P. Markström, A. Lyngfelt, Material balances of carbon, sulfur, nitrogen and ilmenite in a 100 kW CLC reactor system, Int. J. Greenh. Gas Control 27 (2014) 188–202, https://doi.org/10.1016/j.ijggc.2014.05.001.

[40] T. Mattisson, S. Sundqvist, P. Moldenhauer, H. Leion, A. Lyngfelt, Influence of heat treatment on manganese ores as oxygen carriers, Int. J. Greenh. Gas Control 87 (2019) 238–245, https://doi.org/10.1016/J.IJGGC.2019.05.027.

[41] F.J. Velasco-Sarria, A. Abad, I. Adánez-Rubio, A. Abad, J. Adánez, Assessment of low-cost oxygen carrier in South-western Colombia, and its use in the in-situ gasification chemical looping combustion technology, Fuel 218 (2018) 417–424, https://doi.org/10.1016/J.FUEL.2017.11.078.

[42] G. Azimi, H. Leion, T. Mattisson, A. Lyngfelt, Chemical-looping with oxygen uncoupling using combined Mn-Fe oxides, testing in batch fluidized bed, Energy Procedia 4 (2011) 370–377, https://doi.org/10.1016/j.egypro.2011.01.064.

[43] A.L. Golnar Azimi, Magnus Ryeden, Henrik Leion, Tobias Mattisson, (MnzFe1—z)yOx Combined Oxides as Oxygen Carrier for Chemical-Looping with Oxygen Uncoupling, AIChE J. 59 (2013) 582–588, https://doi.org/10.1002/aic.

[44] M. Schmitz, C. Linderholm, Chemical looping combustion of biomass in 10- and 100 kW pilots – analysis of conversion and lifetime using a sintered manganese ore, Fuel 231 (2018) 73–84, https://doi.org/10.1016/j.fuel.2018.05.071.

[45] I. Gogolev, A.H. Soleimanisalim, C. Linderholm, A. Lyngfelt, Commissioning, performance benchmarking, and investigation of alkali emissions in a 10 kW$_{th}$ solid fuel chemical looping combustion pilot, Fuel 287 (2021) 119530, https://doi.org/10.1016/j.fuel.2020.119530.

[46] D. Karami, A.H. Soleimanisalim, M.H. Sedghkerdar, N. Mahinpey, Preparation of Novel Oxygen Carriers Supported by Ti, Zr-Shelled γ-Alumina for Chemical Looping Combustion of Methane, Ind. Eng. Chem. Res. 59 (7) (2020) 3221–3228, https://doi.org/10.1021/acs.iecr.9b06832.